POLITECNICO DI TORINO
Repository ISTITUZIONALE

Improving agricultural drone localization using georeferenced low-complexity maps

Terms of use:

(Article begins on next page)

23 April 2024

Improving agricultural drone localization using georeferenced low-complexity maps

Cesare Donati[1], Martina Mammarella[2], Lorenzo Comba[3,2], Alessandro Biglia[3], Fabrizio Dabbene[2,*], and Paolo Gay[3]

[1] *Department of Computer Engineering – Politecnico di Torino*, Torino, Italy
cesare.donati@studenti.polito.it

[2] *Institute of Electronics, Computer and Telecommunication Engineering, National Research Council of Italy*, Torino, Italy
martina.mammarella@ieiit.cnr.it, fabrizio.dabbene@ieiit.cnr.it

[3] *Department of Agricultural, Forest and Food Sciences (DiSAFA) – Università degli Studi di Torino*, Grugliasco, Italy
lorenzo.comba@unito.it, alessandro.biglia@unito.it, paolo.gay@unito.it

Abstract—To properly locate and operate autonomous vehicles for in-field tasks, the knowledge of their instantaneous position needs to be combined with an accurate spatial description of their environment. In agricultural fields, when operating inside the crops, GPS data are not reliable nor always available, therefore high-precision maps are difficult to be obtained and exploited for in-field operations. Recently, low-complexity, georeferenced 3D maps have been proposed to reduce their computationally demand without losing relevant crop shape information. In this paper, we propose an innovative approach based on the ellipsoid method that allows us to *fuse* the data collected by ultrasonic sensors and the information provided by the simplified map to improve the location estimation of an unmanned ground vehicle within crops. Then, this improved estimation of the vehicle location can be integrated with orientation data, merging it with those provided by other sensors as GPS and IMU, using classical filtering schemes.

Index Terms—Precision farming, position determination, sensor fusion, deterministic filter, ellipsoid method

I. INTRODUCTION

In precision agriculture, autonomous ground and aerial vehicles can lead to favourable improvements to in-field operations, extending crop scouting to large areas and performing field tasks in a timely and effective way [1]. However, automated navigation and operations within a complex scenarios require specific and robust path planning and navigation control [2]. Thus, in addition to a proper knowledge of their instantaneous position, robotic vehicles and machines require an accurate spatial description of the environment. In the autonomous driving framework, several solutions have been proposed, where digital maps data are merged with those obtained by other sensors mounted on the vehicle, e.g. Global Positioning System (GPS), vision-based sensors and Inertial Measurement Unit (IMU).

On the other hand, in the agricultural field, when operating within crops, GPS data are neither reliable nor always available. Indeed, the main disadvantage of this system is that obstacles such as mountains, buildings, and also crop rows can block the GPS signals. Hence, when unmanned vehicles equipped with GPS are operated between vine rows, the possibility to have four satellites visible at once is reduced,

does compromising the GPS effectiveness. In addition, high-precision maps are difficult to be obtained and exploited for in-field operations. Recent studies focused on the development of 3D models [3], using point clouds or triangulated meshes, generated by 3D sensors (e.g., LiDAR [4] and depth cameras [5]) or photogrammetry from structure from motion (SfM) algorithm, processing appropriate sets of 2D images (see e.g., [6], [7]). In agriculture, 3D modelling representations would facilitate comprehension of the environment, allowing to retrieve a set of relevant information regarding crops, such as planting location and canopy shape, crucial for performing tasks within the crops in an autonomous way while guaranteeing collision avoidance [8]. This requires proper algorithms for detecting and mapping crops and identifying soil and obstacles [9], [10]. This task is not trivial since large 3D models of crops, including remotely sensed imagery and measurements made using in-field or on-vehicle sensors, require processing algorithms to process big data and to extract appropriate information depending on the required final goal ([11]). In [12], authors propose a localization approach to estimate the vehicle pose relative to a global navigation satellite system (GNSS)-referenced map of crop rows fusing crop row detections with GNSS signals to obtain a pose estimate with the accuracy comparable to a row-following approach in the heading and lateral offset, while at the same time maintaining at least GNSS accuracy along the row.

However, reducing the amount of data is crucial to reducing computational times for large original datasets, thus enabling the exploitation of high-precision maps or 3D point cloud information in real-time during field operations, rapid communication, and data exchange between in field actors. Hence, innovative modelling framework can be exploited to semantically interpret 3D point clouds of vineyards and to generate low complexity 3D mesh models of vine rows, as the one presented in [13].

Focusing the attention on agricultural unmanned ground vehicles (UGVs), in this paper we propose an innovative approach that allows us to *fuse* the data collected by ultrasonic sensors mounted on the UGV and the information provided by the low-complexity map to improve the estimation of the UGV

location within crops. Then, this more accurate estimation of the UGV location can be further improved and integrated with orientation data merging it with data provided by the other sensors mounted on the UGV itself, i.e. GPS and IMU, using classical filtering schemes, e.g., Kalman filter [14]. The proposed scheme is summarized in Figure 1.
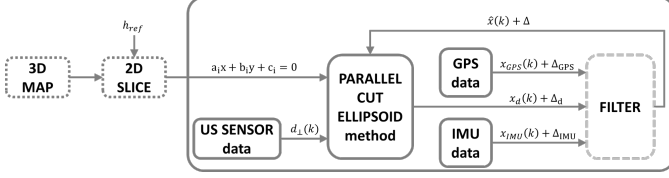

Fig. 1. Given the measured distance $d_\perp(k)$ and the predicted state $\hat{x}(k)$ (affected by an error Δ) at time k, we merge those data with the information provided by the map to update the state $x_d(k)$ and its error Δ_d, later fused with the data coming from GPS and IMU, i.e. x_{GPS} and x_{IMU} respectively, exploiting a filtering scheme to propagate the state estimation at time $k+1$.

We assume that, at every time k, the uncertainty on the UGV position can be modeled with an ellipsoid of the form

$$\mathcal{E}_k = \{x \in \mathbb{R}^n | (x - x_k)^T P_k^{-1}(x - x_k) \leq 1\} \qquad (1)$$

where x_k is the center of $\mathcal{E}_k$ and P_k is a positive semi-definite matrix representing the shape of $\mathcal{E}_k$, i.e. the eigenvectors of P_k define the principal axes of the ellipsoid and its eigenvalues are the reciprocals of the squares of the semi-axes. In the proposed approach, the ellipsoid method [15] is used to merge the distance measured by the ultrasound sensor with the geo-referenced information provided by the low-complexity map to *update* the initial prediction of UGV location, identifying within the initial ellipsoid $\mathcal{E}_k$ of *possible* current positions of the UGV those that are coherent with the sensed distance and the simplified map.

The remainder of the paper is structured as follows. In Section II, an overview on ultrasonic sensor and simplified maps is provided. The parallel cuts method, used to merge sensor and map information is detailed described in Section III. Section IV is dedicated to the presentation of the preliminary results obtained applying the proposed approach to a Nebbiolo vineyard while main conclusions are drawn in Section V.

II. THE SELECTED FRAMEWORK

In this section, we provide an overview of the main elements involved in the data fusion, which are the ultrasonic sensor and the georeferenced low-complexity maps.

A. Ultrasound sensor

Active ranging sensors continue to be the most popular sensors in mobile robotics [16]. They are primarily used for object detection and collision avoidance, but they are also used for *localization*. These range sensors use the time-of-flight (TOF) method: the measured pulses typically come from an ultrasonic, radio-frequency, or optical energy source and the relevant parameters involved in range calculation is the speed of sound in air and the speed of light source. Using elementary physics and geometry, distance can be determined

easily. The measured time is representative of traveling twice the separation distance.

Within this category, we have ultrasonic sensors, which use a transducer to send and receive ultrasonic pulses that relay back information about an object proximity [17] . This type of sensors are commonly mounted on the vehicles to measure the distance between the vehicle and the obstacle to eventually re-plan the mission and to avoid collision.

For UGVs, ultrasonic sensors have been introduced in some studies in combination with Global Positioning System (GPS), vision, and laser range scanner sensors to navigate the mobile robot in different environments, including crops as in [18].

In particular, the ultrasonic sensors provide the distance to the closest obstacle (now approximated as a plane defined by general equation $ax + by + c = 0$), *perpendicularly* to the direction of forward motion of the vehicle itself. This means that, if the (pointmass) UGV in p has a given orientation θ with respect to local frame at time k, the distance d_m measured from p by the sensor, which is supposedly mounted on its side, with respect to an obstacle has an orientation of $\theta' = \theta - \pi/2$.

B. Georeferenced low-complexity map

When autonomous vehicles are called to operate to perform in-field tasks, mapping, modelling and spatial description of the crops play a crucial role. In this context, enhanced performance can be achieved by 3D path planning, which exploits 3D models of the environment. These representations, which can be in the form of point clouds or triangulated mesh, can be generated exploiting different tools. All those methods share one main drawback: the generated dataset are typically vast (and heavy from a memory demand viewpoint) and require (multiple) post-processing steps for extracting valuable information. Moreover, when these datasets are intended to be used in field, the information that can be gathered from on-board sensors, e.g. GPS, are to not enough reliable to be fused with them. For this reason, when considering agricultural scenarios involving UGVs, unsupervised methods to semantically interpret the models and to perform data reduction are key elements in the Agriculture 4.0 framework.

To this aim, an innovative point cloud processing pipeline to automatically detect parcels and vine rows location was proposed in [9] and later exploited in [13] to generate low complexity 3D mesh models of vine rows. The output of the processing flow is made by a reduced set of elements still properly describing the spatial layout and shape of vine, allowing a drastic reduction of the amount of data required without losing relevant crop shape information, as shown in Figure 2(b).

To exploit this map for in-field navigation, we select a reference relative altitude h_{ref} from the terrain with respect to which extrapolate the profile of the row mesh of interest. This h_{ref} refers to the mounting position of the sensors on the UGV with respect to the terrain. Hence, it can be considered fixed. First, we define the plane approximating the terrain, i.e. modelled as $a_t x + b_t y + c_t z + d_t = 0$. Then, we translate this plane by h_{ref} and we intersect our mesh with this plane
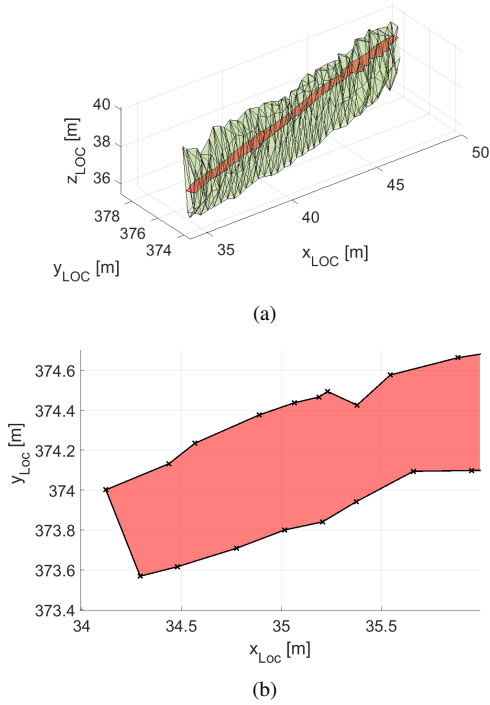
(a)

(b)

Fig. 2. (a) 3D overview of one of the row mesh with the sliced plane (red area) identified at a fixed relative altitude from the terrain. (b) 2D projected slice of the 3D mesh.

obtaining a slice as shown in Figure 2(a). The obtained 2D mesh (red area) is defined by a series of vertices (black crosses in Figure 2(b)), representing the intersecting points among plane and 3D mesh, and segments connecting them, each one defined by the corresponding equation $a_i x + b_i y + c_i = 0$. For the i-th segment, its orientation β_i with respect to the x-axis is defined as

$$\beta_i = \arctan\left(-\frac{a_i}{b_i}\right). \tag{2}$$

This angle will be later used to derive the correlation among the possible UGV location within the ellipsoid $\mathcal{E}_k$, its orientation θ, and $d_\perp$, i.e. the distance from the vehicle to the map defined as

$$d_m = d_\perp + e_d, \tag{3}$$

where e_d is an unknown-but-bounded (UBB) deterministic measurement error.

III. DETERMINISTIC FILTER FOR DATA FUSION

In this section, we provide details on the model used to describe the UGV dynamics and the method selected for propagating the position estimation ellipsoid according to the merged information gathered from the ultrasonic sensor and the simplified map.

A. UGV modelling

For this work, we consider a simplified model for the UGV, described by a double integrator as

$$\ddot{x} = \frac{F_x}{m}, \quad \ddot{y} = \frac{F_y}{m}, \quad \ddot{\theta} = \frac{M}{I_z}, \tag{4}$$

where (x, y, θ) represents the position coordinates and attitude of the UGV in the local frame, respectively, m and I_z are the UGV mass and moment of inertia, respectively. (F_x, F_y) are the control force components and M the control torque with respect to the vehicle z axis. Hence, considering as state vector $\mathbf{x} = [x, y, \theta, \dot{x}, \dot{y}, \dot{\theta}]^\top$ and as input vector $\mathbf{u} = [F_x, F_y, M]^\top$, we have

$$\dot{\mathbf{x}} = A\mathbf{x} + B\mathbf{u} = \begin{bmatrix} 0_{3x3} & \mathbb{I}_3 \\ 0_{3x3} & 0_{3x3} \end{bmatrix} \mathbf{x} + \begin{bmatrix} 0_{3x3} \\ \frac{1}{m} & 0 & 0 \\ 0 & \frac{1}{m} & 0 \\ 0 & 0 & \frac{1}{I_z} \end{bmatrix} \mathbf{u}. \tag{5}$$

This model is later used within the ellipsoid method to propagate the uncertainty ellipsoid $\mathcal{E}_k$, as detailed in the next section.

B. Ellipsoid Method

Since late 1960s, different approaches based on the ellipsoid method have been proposed in the literature, e.g. [19], [20]. Originally, the ellipsoid method was used in optimization to minimize convex functions. Indeed, it allows to generate a sequence of ellipsoids whose volume uniformly decreases at every step, thus enclosing a minimizer of a convex function. The classic formulation is used to obtain the ellipsoid of minimum volume $\mathcal{E}_{k+1}$ which contains all the points in $\mathcal{E}_k$ that also belong to the half-plane passing through its center x_k. In the *deep cut* variant [21], the half-plane is not constrained to pass through the center of the ellipsoid. More recently, [22] provides a different method to find the ellipsoid that tightly bounds the intersection between two given ellipsoids. Another method is described in [23], which allows to use simultaneously the constraints imposed by a pair of *parallel cuts* and to generate the new ellipsoid $\mathcal{E}_{k+1}$ having minimum volume and containing all the points between the two half-spaces (see Figure 3).
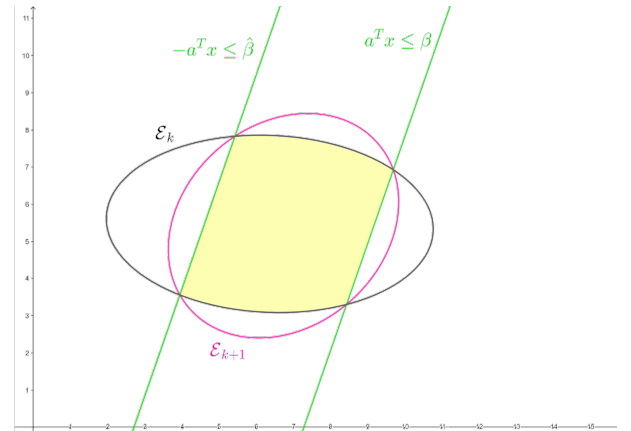

Fig. 3. In the parallel cuts method, two half-plane are considered simultaneously and the minimum volume ellipsoid $\mathcal{E}_{k+1}$ containing the area constrained among the ellipsoid $\mathcal{E}_k$ and the two half-planes (yellow area).

Let us define the parallel cuts as

$$a^T x \leq \beta, \quad -a^T x \leq \hat{\beta}. \tag{6}$$

The algebraic distance of each half-plane from the center of the ellipse x_k can be computed as

$$\alpha = \frac{a^T x_k - \beta}{\sqrt{(a^T P_k a)}}, \quad \hat{\alpha} = \frac{\hat{\beta} - a^T x_k}{\sqrt{(a^T P_k a)}}. \tag{7}$$

Then, we can compute the propagation of the ellipsoid $\mathcal{E}_{k+1}$ by its center x_{k+1} and shape matrix P_{k+1} as

$$x_{k+1} = x_k - \tau \frac{P_k a}{\sqrt{a^T P_k a}}, \quad P_{k+1} = \delta(P_k - \sigma \frac{P_k a (P_k a)^T}{\sqrt{a^T P_k a}}), \tag{8}$$

where n is the space dimension, and σ, τ, δ are the dilation, step and expansion parameters, respectively. In the parallel cuts approach, these parameters can be computed as

$$\sigma = \frac{1}{n+1}\Big[n + \frac{2}{(\alpha - \hat{\alpha})^2}(1 - \alpha\hat{\alpha} - \frac{\rho}{2})\Big], \tag{9a}$$

$$\tau = \frac{\alpha - \hat{\alpha}}{2}\sigma, \tag{9b}$$

$$\delta = \frac{n^2}{n^2 - 1}\Big(1 - \frac{\alpha^2 + \hat{\alpha}^2 - \frac{\rho}{n}}{2}\Big), \tag{9c}$$

where $\rho = \sqrt{4(1-\alpha^2)(1-\hat{\alpha}^2) + n^2(\hat{\alpha}^2 - \alpha^2)^2}$.

This last approach has been selected to propagate the uncertainty ellipsoid when the information gathered from the ultrasound sensor and the map are used to generate the parallel cuts as described in the next section.

C. Feasible points and ellipsoid propagation

As anticipated in the previous sections, at each time step k, we can select the feasible points within $\mathcal{E}_k$ defined by the subset $\mathcal{F} \subseteq \mathcal{E}_k$, i.e.

$$\mathcal{F} = \Big\{p \in \mathcal{E}_k | d_m^{min} \le d_\perp(p) \le d_m^{max}\Big\} \tag{10}$$

where d_m^{min}, d_m^{max} are the minimum and maximum value of the measurement d_m, respectively, defined according to the bounds on e_d, and $d_\perp(p_i)$ is the perpendicular distance computed on the map from the generic point $p_i = (xi, yi) \in \mathcal{E}_k$ with orientation θ_i with respect to the x-axis as

$$d_\perp(p_i) = \frac{d_{min}(p_i)}{cos(\gamma)}, \tag{11}$$

where $d_{min}(p_i)$ is the minimum distance from p_i to the plane (see Figure 4), defined by

$$d_{min}(p_i) = \frac{|ax_i + by_i + c|}{\sqrt{a^2 + b^2}} \tag{12}$$

and $\gamma = \beta - \theta_i$ is the angle between $d_\perp$ and d_{min}. This procedure can be used to estimate the feasible region $\mathcal{F}$ in $\mathcal{E}_k$ from which we can recover the parallel cuts and propagate the ellipsoid itself at the next time step as presented in Section III-B. However, this method could results quite computationally heavy and we propose next a valid alternative that directly

[1]According to the value of α and $\hat{\alpha}$, we have some special cases:
1) if $|\alpha| \ge 1$, then $\alpha = sign(\alpha)$ (equivalently for $\hat{\alpha}$).
2) if $\alpha \cdot \hat{\alpha} \ge \frac{1}{n}$, then $\mathcal{E}_{k+1} = \mathcal{E}_k$.

provides the equation of the two half-spaces starting from the knowledge of the approximating map. Indeed, we can observe that the two half-spaces can be easily defined starting from the reference plane $ax + by + c = 0$ and estimating two offsets d_O^{min} and d_O^{max}.
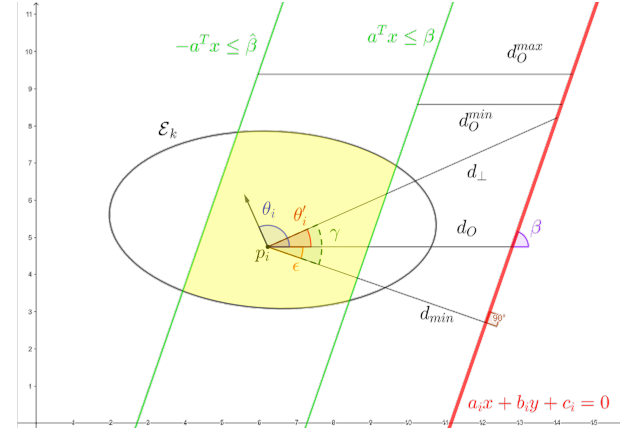

Fig. 4. Given a point p_i in the ellipsoid $\mathcal{E}_k$ and the approximating red line, it is possible to obtain the points in $\mathcal{E}_k$, which distance from the line is compatible with the measured one. These points belongs to the yellow area of $\mathcal{E}_k$, constrained between half-planes $\pm a \le \beta$, which represent the loci of points equidistant ($d_{min} = d_{min}^{min}$ or $d_{min} = d_{min}^{max}$) from $a_i x + b_i y + c_i = 0$.

Going into the details, given a generic point p_i in $\mathcal{E}_k$, its measured offset d_O from the row is defined as

$$d_O(p_i, \theta_i) = \frac{d_{min}(p_i)}{\cos \varepsilon}. \tag{13}$$

where $\varepsilon = \beta - \frac{\pi}{2}$. In this case, the minimum distance from p_i to the row can be computed as $d_{min} = d_\perp \cos\gamma$ and, given the bounds on $d_\perp$ (10), we can obtain the lower and upper bounds for the offset itself as

$$d_O^{min} = \frac{d_m^{min} \cos\gamma}{\cos\varepsilon}, \quad d_O^{max} = \frac{d_m^{max} \cos\gamma}{\cos\varepsilon}, \tag{14}$$

Then, we can recover the definition of the two parallel cuts as follows

$$a = -\frac{a_i}{b_i}, \quad \beta = -\frac{c_i}{b_i} - \frac{a_i}{b_i}d_O^{min}, \quad \hat{\beta} = -\frac{c_i}{b_i} - \frac{a_i}{b_i}d_O^{max}. \tag{15}$$

We are now able to identify at each time step k the feasible region $\mathcal{F}$ in the uncertainty ellipsoid $\mathcal{E}_k$ and to propagate it exploiting the parallel cuts method as described in Section III-B.

D. Sensor fusion

The Ellipsoidal approach adopted in the previous subsection allows to exploit the information coming from the 2D map to construct an ellipsodal estimation of the UGV position. This is then exploited in an ad-hoc designed Kalman-like filter to fuse this information with IMU and GPS signals.

IV. PRELIMINARY RESULTS

The case study involves a vineyard located in Barolo (Piedmont, Italy), which extends over a surface of about 0.7 hectares and its elevation ranges from 460 to 490 m above sea

| Sensor	Parameter	Value
Ultrasonic	Distance range	0.02–0.45 [m]
	Accuracy	3 [mm]
GPS	RTK accuracy	1 [cm] + 1 [ppm]
	SBAS accuracy	0.6 [m]
IMU	Position accuracy	1 [m]
	Velocity accuracy	0.05 [m/s]
	Accelerometer accuracy	200 [m/s^2]
	Gyroscope accuracy	450 [deg/s]

Fig. 5. Comparison among estimation error when only on board sensors are exploited (upper figure) or when they are combined with low-complexity maps (lower figure).
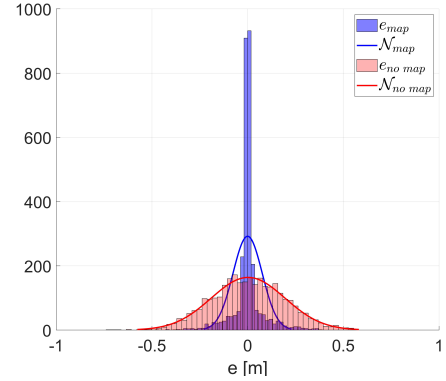

Fig. 6. Histograms for error estimation when maps are combined with on-board sensors (blue) or they are not exploited (red).

level. The space between vine plants and the inter-row space are about 0.9 m and 2.5 m, respectively.

We consider to operate a 4 wheel steering UGV, equipped with HC-SR04 ultrasonic sensors on both its lateral sides, a Novatel OEM7600 receiver GPS, and a XSens MTI-10 series IMU. The main features of the equipped sensors are reported in Table I. For simulation purposes, ultrasonic sensor noise was modelled as a uniform distribution whereas GPS and IMU noise as Gaussian distributions, i.e. in terms of mean value and variance.

In Figure 5, the comparison among the position estimation error obtained fusing only data measured by sensors (ultrasonic, GPS and IMU) with the one got merging the same information with the map is represented. It is possible to observe that in the second case, the average value of the estimation error is significantly reduced, with some exceptions. These anomalies can be attributed to the effect of map linestring corners, which can affect the definition of the distance measurement. Indeed, according to the vehicle orientation, near the corners the ultrasonic sensor can capture one of the two segments and, correspondingly, the resulting position estimate can be more affected by the measurement error.

The effectiveness of the proposed approach is also confirmed by the histograms reported in Figure 6 that highlight the significant reduction of the standard deviation of the error when the maps are exploited.

In Figure 7 it is possible to appreciate the benefits of the proposed filtering approach with respect to a single segment. In this example we provide a comparison between prediction and uncertainties propagation, obtained by a merging the GPS and IMU data with a classic filter (blue ellipses and blue circles), and the ones obtained when the data from ultrasonic sensors and the map are introduced (red ellipses and red crosses).

Last, in Figure 8 we propose an overview of the proposed scheme applied to the selected vineyard where the estimation error ellipsoid (black dotted line) is reduced and approximated with the minimum volume ellipsoid (red line), when the data from the map (green linestring) are fused with those measured by the four ultrasonic sensors.
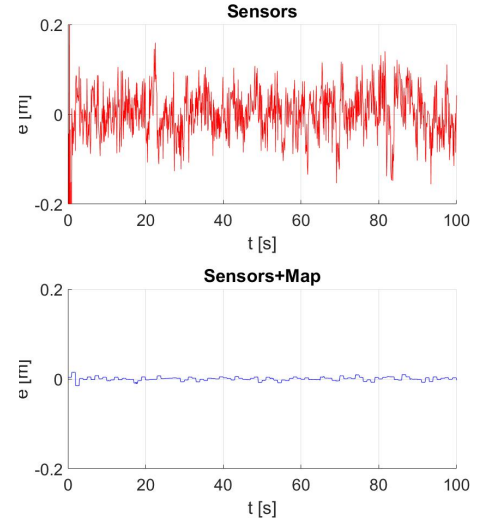
V. MAIN CONCLUSIONS AND FUTURE WORKS

In this paper, we propose an innovative approach, based on the so-called ellipsoid method, to fuse the data provided by the onboard sensors with low-complexity, georeferenced maps, thus improving the estimation of the UGV location when operated within crops. The effectiveness of this scheme has been validated into a simulation setup, considering a 4 wheel steering UGV operated within a Nebbiolo vineyard and equipped with ultrasonic sensors, GPS and IMU board.
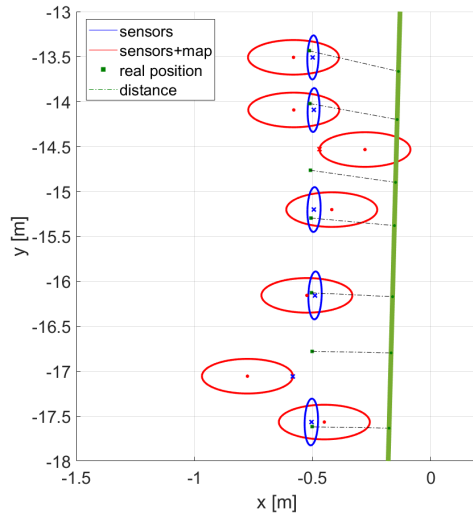
Fig. 7. Vehicle location prediction and related uncertainty ellipsoid when only GPS and IMU are considered (blue) or when maps and ultrasonic sensors are included.
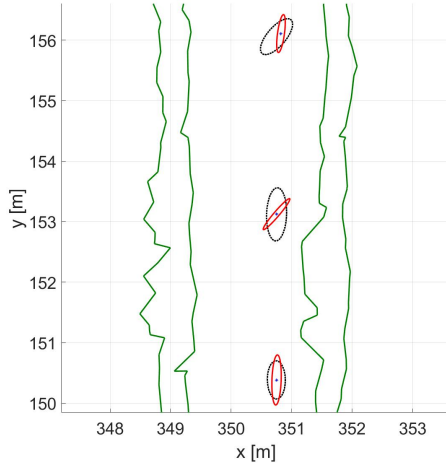

Fig. 8. Evolution of the estimation ellipsoid (black dotted line) and the minimum volume ellipsoid (red line) when data from sensors are fused with the georeferenced information provided by the simplified map of the vine rows (green linestrings).

REFERENCES

[1] D. Rose and J. Chilvers, "Agriculture 4.0: responsible innovation in an era of smart farming," *Frontiers in Sustainable Food Systems*, vol. 2, p. 87, 2018.

[2] M. Mammarella, L. Comba, A. Biglia, F. Dabbene, and P. Gay, "Cooperative agricultural operations of aerial and ground unmanned vehicles," in *2020 IEEE International Workshop on Metrology for Agriculture and Forestry (MetroAgriFor)*. IEEE, 2020, pp. 224–229.

[3] A. Miranda-Fuentes, J. Llorens, J. L. Gamarra-Diezma, J. A. Gil-Ribes, and E. Gil, "Towards an optimized method of olive tree crown volume measurement," *Sensors*, vol. 15, no. 2, pp. 3671–3687, 2015.

[4] J. Mack, C. Lenz, J. Teutrine, and V. Steinhage, "High-precision 3d detection and reconstruction of grapes from laser range data for efficient phenotyping based on supervised learning," *Computers and Electronics in Agriculture*, vol. 135, pp. 300–311, 2017.

[5] I. C. Condotta, T. M. Brown-Brandl, S. K. Pitla, J. P. Stinn, and K. O. Silva-Miranda, "Evaluation of low-cost depth cameras for agricultural applications," *Computers and Electronics in Agriculture*, vol. 173, p. 105394, 2020.

[6] A. Feng, J. Zhou, E. D. Vories, K. A. Sudduth, and M. Zhang, "Yield estimation in cotton using uav-based multi-sensor imagery," *Biosystems Engineering*, vol. 193, pp. 101–114, 2020.

[7] J. Wijesingha, T. Moeckel, F. Hensgen, and M. Wachendorf, "Evaluation of 3d point cloud-based models for the prediction of grassland biomass," *International Journal of Applied Earth Observation and Geoinformation*, vol. 78, pp. 352–359, 2019.

[8] L. Comba, A. Biglia, D. Ricauda Aimonino, P. Barge, C. Tortia, and P. Gay, "Neural network clustering for crops thermal mapping," in *VI International Symposium on Applications of Modelling as an Innovative Technology in the Horticultural Supply Chain Model-IT 1311*, 2019, pp. 513–520.

[9] L. Comba, A. Biglia, D. Ricauda Aimonino, and P. Gay, "Unsupervised detection of vineyards by 3D point-cloud uav photogrammetry for precision agriculture," *Computers and Electronics in Agriculture*, vol. 155, pp. 84–95, 2018.

[10] A. K. Mortensen, A. Bender, B. Whelan, M. M. Barbour, S. Sukkarieh, H. Karstoft, and R. Gislum, "Segmentation of lettuce in coloured 3d point clouds for fresh weight estimation," *Computers and Electronics in Agriculture*, vol. 154, pp. 373–381, 2018.

[11] L. Serazetdinova, J. Garratt, A. Baylis, S. Stergiadis, M. Collison, and S. Davis, "How should we turn data into decisions in agrifood?" *Journal of the Science of Food and Agriculture*, vol. 99, no. 7, pp. 3213–3219, 2019.

[12] W. Winterhalter, F. Fleckenstein, C. Dornhege, and W. Burgard, "Localization for precision navigation in agricultural fields—Beyond crop row following," *Journal of Field Robotics*, vol. 38, no. 3, pp. 429–451, 2021.

[13] L. Comba, S. Zaman, A. Biglia, D. Ricauda Aimonino, F. Dabbene, and P. Gay, "Semantic interpretation and complexity reduction of 3D point clouds of vineyards," *Biosystems Engineering*, vol. 197, pp. 216–230, 2020.

[14] T. Oksanen, M. Linja, and A. Visala, "Low-cost positioning system for agricultural vehicles," in *2005 international symposium on computational intelligence in robotics and automation*. IEEE, 2005, pp. 297–302.

[15] R. G. Bland, D. Goldfarb, and M. J. Todd, "The ellipsoid method: A survey," *Operations research*, vol. 29, no. 6, pp. 1039–1091, 1981.

[16] R. Siegwart, I. R. Nourbakhsh, and D. Scaramuzza, *Introduction to autonomous mobile robots*. MIT press, 2011.

[17] G. A. Demetriou, "A survey of sensors for localization of unmanned ground vehicles (ugvs)." in *IC-AI*. Citeseer, 2006, pp. 659–668.

[18] N. Shalal, T. Low, C. McCarthy, and N. Hancock, "A review of autonomous navigation systems in agricultural environments," *Innovative Agricultural Technologies for a Sustainable Future*, pp. 1–16, 2013.

[19] F. C. Schweppe, "Recursive state estimation: Unknown but bounded errors and system inputs," *6th Symposium on Adaptive Processes, SAP 1967*, pp. 102–107, 1967.

[20] E. Fogle and Y. F. Huang, "On the Value of Information in System Identification-Bounded Noise Case," *Automatica, Vol. 18, No. 2, pp. 229–238. 1982*, vol. 18, no. 2, pp. 229–-238, 1982.

[21] J. B. G. Frenk, J. Gromicho, and S. Zhang, "A deep cut ellipsoid algorithm for convex programming: Theory and applications," *Mathematical Programming*, vol. 63, no. 1, pp. 83–108, 1994.

[22] L. Ros, A. Sabater, and F. Thomas, "An Ellipsoidal Calculus based on propagation and fusion," *IEEE Transactions on Systems, Man, and Cybernetics, Part B: Cybernetics*, vol. 32, no. 4, pp. 430–442, 2002.

[23] A. Liao and M. J. Todd, "The ellipsoid algorithm using parallel cuts," *Computational Optimization and Applications*, vol. 2, no. 4, pp. 299–316, 1993.